IOPscience iopscience.iop.org

Home Search Collections Journals About Contact us My IOPscience

Frequency adjustment of microelectromechanical cantilevers using electrostatic pull down

This content has been downloaded from IOPscience. Please scroll down to see the full text.

2005 J. Micromech. Microeng. 15 1033

(http://iopscience.iop.org/0960-1317/15/5/020)

View the table of contents for this issue, or go to the journal homepage for more

Download details:

IP Address: 142.3.100.23
This content was downloaded on 07/09/2015 at 01:11

Please note that terms and conditions apply.

INSTITUTE OF PHYSICS PUBLISHING JOURNAL OF MICROMECHANICS AND MICROENGINEERING
J. Micromech. Microeng. **15** (2005) 1033–1039 doi:10.1088/0960-1317/15/5/020

Frequency adjustment of microelectromechanical cantilevers using electrostatic pull down

S M M Kafumbe[1], J S Burdess[2] and A J Harris[3]

[1] Institute for Nanoscale Science and Technology, Herschel Building—Annex, University of Newcastle upon Tyne, NE1 7RU, UK
[2] School of Mechanical and Systems Engineering, Stephenson Building, University of Newcastle upon Tyne, NE1 7RU, UK
[3] School of Electrical, Electronic and Computer Engineering, Merz Court, University of Newcastle upon Tyne, NE1 7RU, UK

E-mail: s.m.m.kafumbe@newcastle.ac.uk, j.s.burdess@newcastle.ac.uk and alun.j.harris@newcastle.ac.uk

Received 11 November 2004, in final form 4 March 2005
Published 8 April 2005
Online at stacks.iop.org/JMM/15/1033

Abstract
In this paper, a new way of actively tuning the resonant frequency of vibrating microelectromechanical devices by electrostatically adjusting the length of the resonating structure is explored. Variations in micromachining processes cause submicron differences in the size of fabricated micromachined devices, which lead to frequency variations in resonators. For radio frequency (RF) applications where high frequency selectivity and low noise frequency manipulation are key performance issues, micromachined resonators need to output a fixed frequency if they are to replace current off-chip, passive devices. This motivates the investigation of post-fabrication techniques that compensate for fabrication defects and errors, and shift the resonant frequency to its designed value. A simple universal analytical model has been developed to investigate the different states a cantilever undergoes during pull-in due to an applied voltage. The beam's natural frequencies throughout these states have been plotted. It is shown that the frequency can be changed by a factor of 4 during pull down, and thereafter increased proportionally with actuation provided an initial minimum voltage was applied.

1. Introduction

Resonant devices fabricated using high aspect-ratio lithographic and other precision micromachining techniques are used as mechanical sensors for detecting physical and environmental parameters [1, 2]. Additionally, high-Q micromechanical resonators are replacing bulky, off-chip, passive devices in radio frequency (RF) filters, mixers and oscillators used in super-heterodyne wireless transceivers [3–5].

In each of these applications however, there is a need for post fabrication modifications to increase yield, and produce devices to design specifications. This tuning is done to compensate for local process variations, as well as errors and defects occurring during fabrication, which result in a shift or distribution of the resonance frequency. Post fabrication modifications also compensate for environmental factors like ageing [6], contamination [7] and thermal mismatch that could affect the device during its lifetime.

Previous frequency tuning methods relied on changing either the stiffness, or the mass of the resonating device. One way of doing this was by dimensionally trimming the resonator structure using laser [8, 9], reactive ion etching (RIE) and ion milling [10], or focused ion beam micromachining [11]. The other was by selectively depositing polysilicon on well-demarcated regions of the vibrating structure. This was done using laser writing [12], epitaxial growth [13] and by decomposing silane on electrically heated released

0960-1317/05/051033+07$30.00 © 2005 IOP Publishing Ltd Printed in the UK

structures [14, 15]. Inducing stresses in the device also changes its effective stiffness, and therefore the resonating frequency. This was done electrostatically using in-built capacitive actuators [16–18], and electrothermally by passing a current to generate tensile and compressive thermal stresses [19–21].

The active tuning method demonstrated in this paper achieves very large frequency shifts from small changes in the length of the vibrating structure using an actuation voltage. The vibrating structure in this method is a cantilever that is transformed into a clamped–clamped beam after pull down. The large frequency change with length during actuation, over a wide band of frequencies, compares highly to reported figures. These include frequency shifts of 1.9% at around 86.6 kHz using selective deposition [14, 15], 5% at around 650 Hz using focused ion beam micromachining [11] and 6.5% at 31 kHz using electro-thermal stiffness change [19]. Additionally, this method guarantees frequency tuning throughout the lifetime of the device, and overcomes several drawbacks imposed by previous methods. These include high processing temperatures, permanent deformation of the device, large costs of laser equipment required to achieve high precision on nano-scale structures, parasitic capacitances of in-built actuators and non-linear effects like levitation [16] and stiffness hardening [17].

This paper focuses on a novel tuning method that uses actuation voltages to alter the free length of a cantilever beam, and therefore its frequency. In section 2, the theoretical background to the pull-in phenomena is briefly explained. Section 3 then discusses the different states that a cantilever undergoes during electrostatic actuation together with plots of the frequency response of the beam with increasing and decreasing voltages. Section 4 gives a discussion on the different states, and their implications to frequency tuning. Stiction resulting from van der Waals and other surface adhesion effects after contact has been extensively analysed [22–26]. This can be reduced during device fabrication by using anti-stiction coatings [27], increasing the surface roughness [28], and by designing dimples in the cantilever and spacer posts or sidewalls on the landing bottom layer [29, 30]. In this analysis, the work done by stiction forces is assumed small as compared to the necessary elastic deformation energy of the cantilever. Also, fringing effects are neglected throughout the analysis.

2. Theory

In elastic systems which are strained as the result of electrostatic actuation [31–33], pull-in arises as the final consequence of the build up of electrostatic forces, due to the increased proximity of neighbouring charges opposing the resorting action of elastic forces. To understand how this phenomenon can be exploited to achieve the frequency control of a cantilever beam, consider the situation shown in figure 1. Here a cantilever of density ρ, Young's modulus E, original length L_0, width b and thickness d is initially separated from an electrode by an electrostatic gap H with free space permittivity ε_0. To avoid a short circuit on pull down, a landing insulating layer of thickness h and permittivity ε_1 is placed on the electrode.

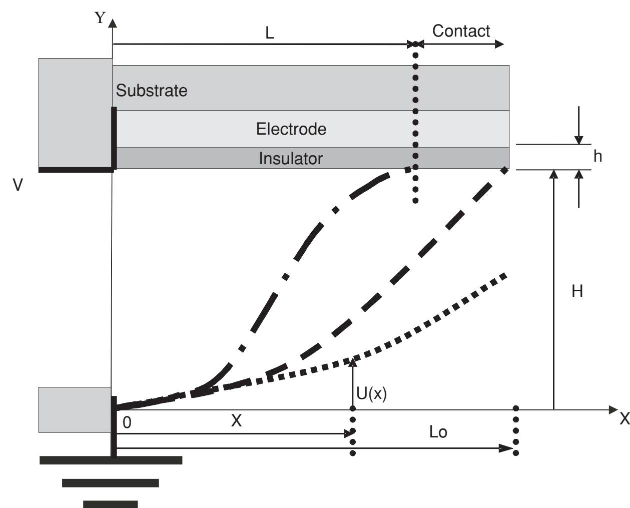

Figure 1. System configuration and states. State 1 is represented by (· · · · · ·), state 2 by (- - - -) and state 3 by (— · —).

When an external voltage V is applied across the cantilever and the electrode, an attracting electrostatic force is produced. Initially, it pulls the cantilever into a deflection profile $u(x)$, as shown by state 1. In this state the natural frequency of free vibration will be determined by the characteristics of the cantilevered form. At a critical value of V this form becomes statically unstable, and it is postulated that the beam thereafter moves to a different equilibrium state, identified as state 2 in figure 1. For state 2, the end of the beam contacts the surface of the insulation, and maintains an end displacement of H. Here, the natural frequency will be determined by the characteristics of a clamped–pinned beam of length, L_0. When the voltage is increased further it is supposed that the end region of the beam rotates towards the insulation until a second critical value is reached. Thereafter the end portion of the beam conforms with the surface of the insulation, and the free length of the beam is reduced to L in state 3. The natural frequency is now determined by the characteristics of a clamped–clamped beam.

A static and dynamic analysis of these states will now be carried out for increasing and decreasing values of voltage. The critical voltages, and the manner in which the first natural frequency of the beam varies with applied voltage, will be determined.

3. Analysis of states 1–3

3.1. State 1

The equations which determine the dynamic behaviour of the cantilever before pull-in occurs can be derived from Hamilton's principle [34, 35] by setting the Lagrangian L_a, as

$$L_a = T - V_b + V_c \tag{1}$$

where the kinetic energy T and the strain energy of the cantilever V_b are

$$T = \frac{\rho b d L_0 H^2}{2 p_1{}^2} \int_0^1 \left(\frac{\partial u}{\partial \tau}\right)^2 \, d\mu; \tag{2}$$

$$V_{\mathrm{b}} = \frac{Ebd^3H^2}{24{L_0}^3}\int_0^1 \left(\frac{\partial^2 u}{\partial \mu^2}\right)^2 \mathrm{d}\mu; \tag{3}$$

and the electrical energy stored by the capacitor formed by the beam and the electrode, V_{c}, is

$$V_{\mathrm{c}} = \frac{\varepsilon_0 V^2 b L_0}{2H}\int_0^1 \left(\frac{1}{1+h/H-u}\right)\mathrm{d}\mu. \tag{4}$$

Here, the non-dimensional beam displacement u and space variable μ are defined as $u = U/H$ and $\mu = x/L_0$, respectively. The non-dimensional time is given by $\tau = p_1 t$, where p_1 is the first natural frequency of the non-actuated cantilever. Minimization of the Lagrangian with respect to the displacement u gives the motion of the cantilever and the boundary conditions as

$$\frac{\partial^4 u}{\partial \mu^4} - \frac{6\Gamma^2}{(1+h/H-u)^2} + \lambda^4\frac{\partial^2 u}{\partial \tau^2} = 0, \tag{5}$$

$$u|_{\mu=0} = \left.\frac{\partial u}{\partial \mu}\right|_{\mu=0} = 0, \tag{6}$$

$$\left.\frac{\partial^2 u}{\partial \mu^2}\right|_{\mu=1} = \left.\frac{\partial^3 u}{\partial \mu^3}\right|_{\mu=1} = 0, \tag{7}$$

where

$$\Gamma^2 = \frac{\varepsilon_0 V^2 {L_0}^4}{Ed^3H^3}, \tag{8}$$

and

$$\lambda^4 = \frac{12{p_1}^2\rho {L_0}^4}{Ed^2}. \tag{9}$$

The solution of equations (5), (6) and (7) now proceeds in two stages. In the first stage $\partial/\partial\tau = 0$, and the static solution $u = u_0(\mu)$ is determined by numerical integration of (5) using a MATLAB routine [36, 37]. For the second stage, (5) is linearized by setting $u = u_0(\mu) + \nu(\mu,\tau)$, where $\nu(\mu,\tau)$ is assumed to be a perturbation of the cantilever's displacement about the static state $u = u_0(\mu)$. The equations which determine $\nu(\mu,\tau)$ are

$$\frac{\partial^4 \nu}{\partial \mu^4} - \left[\frac{12\Gamma^2}{(1+h/H-u_0(\mu))^3}\right]\nu + \lambda^4\frac{\partial^2 \nu}{\partial \tau^2} = 0; \tag{10}$$

$$\nu|_{\mu=0} = \left.\frac{\partial \nu}{\partial \mu}\right|_{\mu=0} = 0; \tag{11}$$

and

$$\left.\frac{\partial^2 \nu}{\partial \mu^2}\right|_{\mu=1} = \left.\frac{\partial^3 \nu}{\partial \mu^3}\right|_{\mu=1} = 0. \tag{12}$$

The natural frequencies, and thus the pull-in stability of the system will be determined by the eigenvalues of (10). To determine the natural frequencies of the cantilever, a solution of the form

$$\nu(\mu,\tau) = \left[\sum_{k=1}^{N}\alpha_k\phi_k(\mu)\right]\sin(r\tau) \tag{13}$$

is sought, where α_k and r are the factors to be determined. The functions $\phi_k(\mu)$ are the mode shapes of the non-actuated cantilever [38], given by

$$\phi_k(\mu) = [\cosh(\beta_k\mu) - \cos(\beta_k\mu)] - \left[\frac{\sinh(\beta_k) - \sin(\beta_k)}{\cosh(\beta_k) - \cos(\beta_k)}\right][\sinh(\beta_k\mu) - \sin(\beta_k\mu)], \tag{14}$$

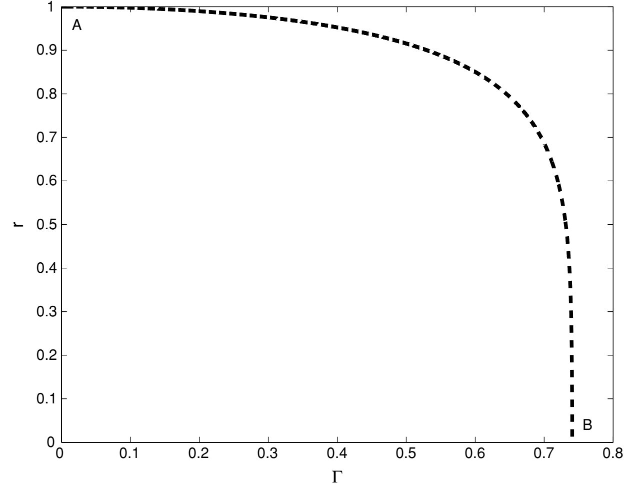

Figure 2. Variation of normalized frequency with the normalized actuation voltage from the unactuated point A to the critical point B where $\Gamma = \Gamma_{c1} \approx 0.7407$ for the case when $h/H = 0.25$.

and satisfy the boundary conditions (11) and (12), as well as the orthogonal conditions (15) and (16):

$$\int_0^1 \phi_i\phi_j\,\mathrm{d}\mu = \delta_{ij}; \tag{15}$$

$$\int_0^1 \frac{\partial^2\phi_i}{\partial\mu^2}\frac{\partial^2\phi_j}{\partial\mu^2}\,\mathrm{d}\mu = {\beta_i}^4\delta_{ij}. \tag{16}$$

Here β_k are the roots of the frequency equation [38]

$$\cosh(\beta_k)\cos(\beta_k) + 1 = 0. \tag{17}$$

When (13) is substituted into (10), and Galerkin's procedure [39, 40] applied, a standard eigenvalue problem,

$$\sum_{k=1}^{N}\left[\left({\beta_i}^4 - r^2\lambda^4\right)\delta_{ij} - \Lambda_{ij}\right]\alpha_j = 0, \tag{18}$$

is formed where

$$\Lambda_{ij} = 12\Gamma^2\int_0^1 \frac{\phi_i(\mu)\phi_j(\mu)}{(1+h/H-u_0(\mu))^3}\,\mathrm{d}\mu. \tag{19}$$

The solution of (18) yields r and α_k, and hence the natural frequencies and mode shapes of the actuated cantilever. For the stability of the deflected shape $u_0(\mu)$, all the eigenvalues r must be real, and the condition for the pull-in to just occur is $r = 0$. If a single mode expansion for $\nu(\mu,\tau)$ is assumed i.e. $N = 1$ in (13), and $\lambda = \beta_1$, the first natural frequency and the pull-in condition are given by

$$r^2 = \frac{{\beta_k}^4 - \Lambda_{ij}}{\lambda^4} = 1 - \frac{\Lambda_{ij}}{\beta_k^4}, \tag{20}$$

and

$${\Gamma_{c1}}^2 = {\beta_i}^4\left[12\int_0^1 \frac{\phi_i(\mu)\phi_j(\mu)}{[1+h/H-u_0(\mu)]^3}\,\mathrm{d}\mu\right]^{-1}. \tag{21}$$

Using (20), together with the computed values of $u_0(\mu)$, r is plotted as a function of the actuation number Γ as shown in figure 2, for the case of $h/H = 0.25$. As Γ (proportional to the voltage V) is increased, the frequency number r monotonically decreases along the curve $A \to B$ until at the critical value B, $\Gamma_{c1} \approx 0.7407$, it becomes zero.

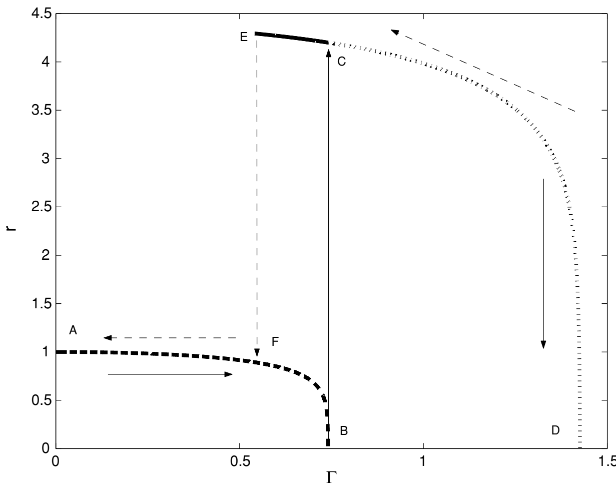

Figure 3. Normalized frequency variation with both increasing ($A \to B \to C \to D$), and decreasing normalized actuation voltage ($D \to E \to F \to A$) for the states 1 (- - - -) and 2 (· · · · · · and ——). The critical values for the case when $h/H = 0.25$ are Γ_{c1} at B, Γ_{c2} at D and Γ_{c3} at E.

3.2. State 2

When $\Gamma > \Gamma_{c1}$, state 1 is unstable, and it is assumed that the beam moves to state 2 as shown in figure 1. Here, the end of the beam makes contact with the insulation. The equation which determines the behaviour of the beam is the same as (5) but the boundary conditions change, and are now given by

$$u|_{\mu=0} = \left.\frac{\partial u}{\partial \mu}\right|_{\mu=0} = 0; \tag{22}$$

$$u|_{\mu=1} = 1; \qquad \left.\frac{\partial^2 u}{\partial \mu^2}\right|_{\mu=1} = 0. \tag{23}$$

There is also the further condition that contact (shear) force acting on the beam at the end $\mu = 1$ must be directed along the surface normal at the point of contact. This condition requires $\partial^3 u/\partial \mu^3 > 0$. The solution to (5), (22) and (23) uses the same procedure as described in state 1 but with the functions $\phi_k(\mu)$, in (13), replaced by the mode shape functions of a clamped–pinned beam,

$$\begin{aligned}\phi_k(\mu) &= \cosh(\beta_k\mu) - \cos(\beta_k\mu)\\ &\quad - \cot(\beta_k)[\sinh(\beta_k\mu) - \sin(\beta_k\mu)]\end{aligned} \tag{24}$$

where β_k is now the solution to

$$\tan(\beta_k) - \tanh(\beta_k) = 0. \tag{25}$$

Calculation of the frequency number, r, for values of $\Gamma > \Gamma_{c1}$ shows (figure 3, for the case of $h/H = 0.25$) that r 'jumps' from $r = 0$ at B to the value $r = 4.1997$ at C, and thereafter decreases to zero again at D, when $\Gamma = \Gamma_{c2} = 1.4258$. If it is now assumed that r is at C, and instead of increasing the value of Γ, it is reduced, then it is noted that the condition remains satisfied until Γ is reduced to the third critical value $\Gamma = \Gamma_{c3} = 0.5408$. At this point the condition $\partial^3 u/\partial \mu^3 > 0$ becomes violated, and it is implied that contact at the tip of the beam is lost. The beam thus returns to state 1, r 'jumps' from E to F, and thereafter follows the curve $F \to A$.

3.3. State 3

Suppose Γ is increased from zero, and reaches values $\Gamma > \Gamma_{c2}$. For these values it is assumed that the cantilever takes up the static shape shown by state 3 in figure 1. Here the end portion of the cantilever becomes attached to the insulation, and the free region is of unknown span $\eta = L/L_0 \leqslant 1$. To analyse this situation it is necessary to reformulate the Lagrangian, and for this case the energy terms are

$$T = \frac{\rho b d L_0 H^2}{2{p_1}^2}\int_0^\eta \left(\frac{\partial u}{\partial \tau}\right)^2 \mathrm{d}\mu, \tag{26}$$

$$V_\mathrm{b} = \frac{Ebd^3H^2}{24{L_0}^3}\int_0^\eta \left(\frac{\partial^2 u_0}{\partial \mu^2}\right)^2 \mathrm{d}\mu, \tag{27}$$

and

$$V_\mathrm{c} = \frac{\varepsilon_0 V^2 b L_0}{2H}\int_0^\eta \left(\frac{1}{1 + h/H - u}\right)\mathrm{d}\mu + \frac{\varepsilon_0 V^2 b L_0}{2h}(1-\eta). \tag{28}$$

The variation of the Lagrangian $L_\mathrm{a} = T - V_\mathrm{b} + V_\mathrm{c}$, which is now calculated with respect to the variations δu and $\delta\tau$, can be written as

$$\begin{aligned}\delta L_a = \int_0^\eta &\left[-\rho b d L_0 {p_1}^2 \frac{\partial^2 u}{\partial \tau^2} - \frac{Ebd^3H^2}{12{L_0}^3}\frac{\partial^4 u_0}{\partial \mu^4}\right.\\ &\left. + \frac{\varepsilon_0 V^2 b L_0}{2H(1 + h/H - u)^2}\right]\delta u \,\mathrm{d}\mu\\ &+ \frac{Ebd^3H^2}{24{L_0}^3}\left.\left(\frac{\partial^2 u}{\partial \mu^2}\right)^2\right|_{\mu=\eta}\delta\eta.\end{aligned} \tag{29}$$

Here it has been assumed that the variations of u and $\partial u/\partial\tau$ at the end points $(0, \eta)$ are zero, and that the following boundary conditions are satisfied:

$$u|_{\mu=(0,\eta)} = \left.\frac{\partial u}{\partial \mu}\right|_{\mu=(0,\eta)} = 0. \tag{30}$$

The requirement $\delta L_a = 0$ thus gives

$$\frac{\partial^4 u}{\partial \mu^4} - \frac{6\Gamma^2}{(1 + h/H - u)^2} + \lambda^4\frac{\partial^2 u}{\partial \tau^2} = 0, \tag{31}$$

and

$$\left.\frac{\partial^2 u}{\partial \mu^2}\right|_{\mu=\eta} = 0. \tag{32}$$

It will be noted that (32) is an additional requirement, and provides the condition which determines the value of the contact position, η. In their present form, equations (30), (31) and (32) are difficult to solve as condition (32) is not easily accommodated into the method used in state 1. To overcome this, (31) is transformed into an integral by making use of the relationship

$$\begin{aligned}&\int_0^\mu \ldots n \text{ times} \ldots \int_0^\mu F(\sigma)\,\mathrm{d}\sigma\\ &= \int_0^\mu \frac{(\mu-\sigma)^{(n-1)}}{(n-1)!}F(\sigma)\,\mathrm{d}\sigma + \sum_{j=0}^{n-1}\frac{A_j}{j!}\mu^j,\end{aligned} \tag{33}$$

where A_j are arbitrary constants. For this case $n = 4$, so

$$F(\mu) = \frac{\partial^4 u}{\partial \mu^4} = \frac{6\Gamma^2}{(1 + h/H - u)^2} - \lambda^4\frac{\partial^2 \nu}{\partial \tau^2}, \tag{34}$$

and the constants $A_0 \dots A_3$ are found by applying the boundary conditions in (30). By following this procedure, it follows that condition (31) can be written in the integral form

$$\int_0^{\eta} \left[\frac{\sigma^2(\eta - \sigma)}{6} \left(\frac{6\Gamma^2}{(1 + h/H - u)^2} - \lambda^4 \frac{\partial^2 u}{\partial \tau^2} \right) \right] \mathrm{d}\sigma = 1. \tag{35}$$

A solution is now sought by following the linearization procedure outlined in (5), (6) and (7) by rewriting the displacement as $u = u_0 + \nu$, and the free length $\eta = \eta_0 + \gamma$. Here (u_0, η_0) represents the static state of the beam, whereas (ν, γ) represents the small dynamic perturbations. If the Taylor expansion $f(\eta) = f(\eta_0) + \gamma \partial f/\partial \mu|_{\mu=\eta_0} + \cdots$ is used then equations (30), (31) and (35) can be re-written to a first order in ν and γ. For the static solution:

$$\frac{\partial^4 u_0}{\partial \xi^4} - \frac{6K^2}{(1 + h/H - u_0(\mu))^2} = 0; \tag{36}$$

$$u_0|_{\xi=(0,1)} = \left.\frac{\partial u_0}{\partial \xi}\right|_{\xi=(0,1)} = 0; \tag{37}$$

where

$$K^2 = \Gamma^2 \eta_0 = \left[\int_0^1 \frac{\sigma^2(1 - \sigma)}{(1 + h/H - u_0)^3} \mathrm{d}\sigma \right]^{-1}. \tag{38}$$

For the dynamic solution,

$$\frac{\partial^4 \nu}{\partial \xi^4} - \frac{12K^2}{[1 + h/H - u_0(\mu)]^3} \nu + \lambda^4 \eta_0{}^4 \frac{\partial^2 \nu}{\partial \tau^2} = 0; \tag{39}$$

$$\nu|_{\xi=(0,1)} = \left.\frac{\partial \nu}{\partial \xi}\right|_{\xi=(0,1)} = 0; \tag{40}$$

and

$$\gamma = \eta_0 \int_0^1 \sigma^2(1 - \sigma) \left[\lambda^4 \frac{\partial^2 \nu}{\partial \tau^2} - \frac{12\Gamma^2 \nu}{(1 + h/H - u_0(\mu))^3} \right] \mathrm{d}\sigma \times \left(\int_0^1 \frac{12\Gamma^2 \sigma^2}{(1 + h/H - u_0(\mu))^2} \mathrm{d}\sigma \right)^{-1}. \tag{41}$$

In the above equations, the space variable μ has been rescaled according to $\mu = \eta_0 \xi$. This has the advantage of redefining integrals (38) and (41) over the fixed range, (0,1). To solve for u_0 and η_0, the following iterative procedure was used. An initial trial function $u_0{}^{(0)}(\xi)$ was proposed, and an estimate for K, $K^{(0)}$, found from (38). This estimate was then substituted into (36), and solved numerically to satisfy (37). The resulting solution thus provided an updated trial function $u_0^{(1)}$, and the foregoing procedure was repeated until convergence occurred. A flow diagram of the iteration scheme is shown in figure 4. It is assumed here that convergence will occur, and by satisfying (32) using (35) and (36), the iteration provides a method which is more tolerant of the initial form chosen for $u_0(\xi)$. To illustrate the effectiveness of this procedure two trial functions were examined: (i) $u_0^{(0)} = \xi$, and (ii) $u_0^{(0)} = [1 - \cos(\pi\xi)]/2$. Both trial functions converged to the same deflection profile as shown in figure 5, and gave $K = 1.3917$ when $h/H = 0.25$.

The MATLAB boundary-value numerical routine used for this solution [36, 37] produces $\partial^2 u_0/\partial \xi^2$ as an output, and for the fully iterated case, its value at $\xi = 1$ was shown to satisfy (32), as shown in figure 6.

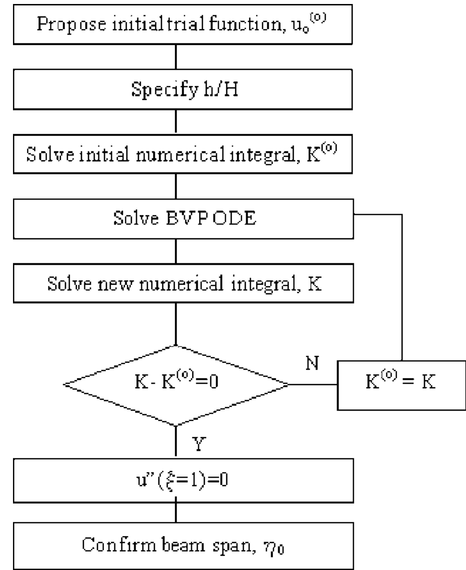

Figure 4. Iterative coupled electrostatic solution analysis methodology.

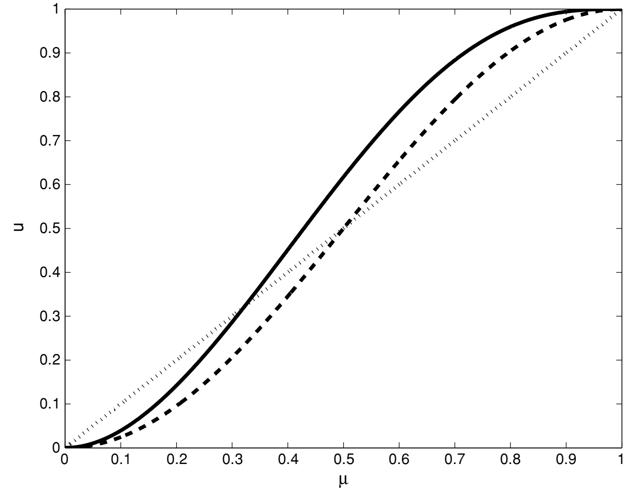

Figure 5. Comparing the final deflection for both initial trial functions. The trial function (i) $u_0^{(0)} = \xi$ is represented by (······), the trial function (ii) $u_0^{(0)} = [1 - \cos(\pi\xi)]/2$ by (- - - -) and the convergent solution by (——).

The free span of the beam can now be calculated from (35), and is given by the simple expression $\eta_0 \approx \sqrt{K/\Gamma}$. For the special case where $h/H = 0.25$, $\Gamma > \Gamma_{c2} = 1.4258$ and $\eta_0 = 0.988$. This shows that the free length of the beam is reduced. Once u_0 has been determined, equations (39), (40) and (41) can be solved using Galerkin's procedure [39, 40], by assuming the form given by (13). For this case the function $\phi_k(\mu)$ is given by the mode shape functions of a clamped–clamped beam

$$\phi_k(\mu) = \cosh(\beta_k \mu) - \cos(\beta_k \mu) - \left[\frac{\cosh(\beta_k) - \cos(\beta_k)}{\sinh(\beta_k) - \sin(\beta_k)} \right] [\sinh(\beta_k \mu) - \sin(\beta_k \mu)], \tag{42}$$

where β_k satisfies

$$\cosh(\beta_k) \cos(\beta_k) = 1. \tag{43}$$

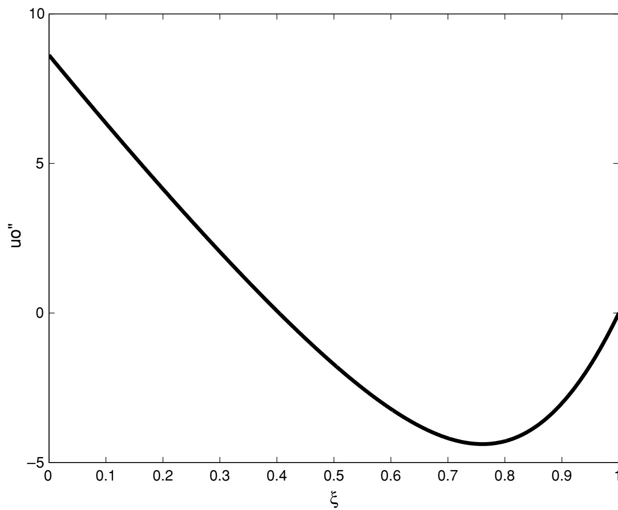

Figure 6. Verifying the beam curvature at the last contact point with the substrate defined when $\xi = 1$.

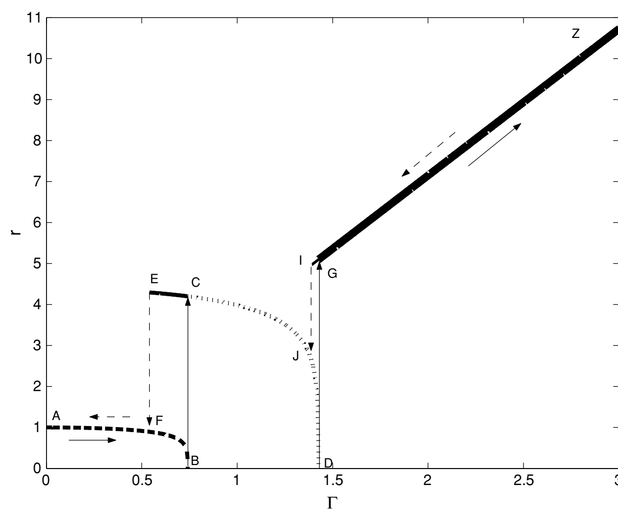

Figure 7. Normalized frequency variation with both increasing ($A \to B \to C \to D \to G \to Z$), and decreasing normalized actuation voltage ($Z \to I \to J \to E \to F \to A$) for the states 1 (- - - -), 2 (······ and ——) and 3 (——). The critical values for the case when $h/H = 0.25$ are Γ_{c1} at B, Γ_{c2} at D, Γ_{c3} at E and Γ_{c4} at I.

If the simple single mode expansion of $v(\mu, \tau)$ is used, the frequency number is found from (18) and can be written as

$$r^2 \approx \frac{\Gamma^2}{\lambda^4}\left[\frac{\beta_i^4}{K^2} - 12\int_0^1 \frac{\phi_i(\mu)\phi_j(\mu)}{[1 + h/H - u_0(\mu)]^3\,\mathrm{d}\mu}\right]^2. \quad (44)$$

Equation (44) shows that the frequency number increases proportionally with Γ, as represented in figure 7 by the line $G \to Z$. When Γ is reduced from its value at Z, r at first follows $Z \to G$ but after G, it continues in a proportional manner until point I is reached when $\Gamma_{c4} = K = 1.3917$ for the case of $h/H = 0.25$. For this value of Γ, $\eta_0 = 1$ and the beam adopts the clamped–pinned configuration. Further reduction in the values of Γ causes r to follow the path $I \to J \to E \to F \to A$.

4. Discussion

4.1. Increasing voltage

Before any voltage is applied, the normalized fundamental frequency number of the cantilever is defined by point A, and is $r = 1$. An increase in voltage produces a proportional increase in the actuation number Γ, and the cantilever is attracted towards the insulating layer. The electrostatic actuation causes the cantilever to suffer a loss of stiffness, and the frequency number is lowered from A to zero at B, when $\Gamma = \Gamma_{c1}$. For values of $\Gamma > \Gamma_{c1}$, pull-in occurs and the cantilever adopts the state corresponding to a clamped–pinned beam. Immediately after pull-in the frequency number undergoes a step change, and takes a value defined by point C. Further increases in Γ cause r to adopt values along the curve $C \to D$, and become zero at $\Gamma = \Gamma_{c2}$. Further actuation renders the cantilever–pinned state of the beam unstable, and the beam takes up a clamped–clamped configuration, with the end region conforming to the surface of the insulating layer. In this state the frequency number undergoes a step change from $D \to G$, and the free length is reduced. Thereafter, increased values of Γ, say to Z, produce a proportional increase in r.

4.2. Decreasing voltage

When the voltage is reduced from its value at Z, the frequency number retraces its path to point G. A further reduction in Γ does not cause the beam to move to the cantilever–pinned state as the condition $\eta_0 < 1$ remains valid until point I is reached at $\Gamma = \Gamma_{c4}$. Here the clamped–clamped state becomes unstable, the beam moves to the stable clamped–pinned state and the frequency is lowered to point J. Decreasing the voltage further increases the frequency number beyond point C to E, where $\Gamma = \Gamma_{c3}$, and the beam tip detaches from the insulating layer. At this point the beam becomes a cantilever, and the frequency number decreases abruptly to point F. Thereafter further decreases in the voltage cause an increase in the frequency number. When point A is reached the beam is restored to its original unloaded state.

4.3. Frequency tuning

For the purposes of tuning the frequency of the beam it is useful that changes in applied voltage produce a proportional change in frequency. It is therefore desirable to operate only over the $I \leftrightarrow G \leftrightarrow Z$ portion of the r versus Γ characteristic. The initial actuation must therefore be large enough to bring the state of the beam to point G, and thereafter must not exceed the breakdown voltage of the insulating layer. Although the frequency of the beam is independent of the original length of the cantilever between points I and Z, the original length is an important factor as it will determine the minimum value of the voltage and the frequency range of the system.

5. Conclusion

A universal analytical model has been developed to investigate the behaviour of an actuated cantilever before and after pull-in instability. Four critical voltages are derived, and it is shown that these determine the three stable states of the beam. It is

shown that a minimum voltage must be applied to the beam before proportional changes in frequency can be achieved.

References

[1] Aikele M, Bauer K, Ficker W, Neubauer F, Prechtel U, Schalk J and Seidel H 2001 Resonant accelerometor with self-test *Sensors Actuators* A **92** 161–7

[2] Lemkin M and Boser B 1999 A three-axis micromachined accelerometer with a CMOS position-sense interface and digital offset-trim electronics *IEEE J. Solid-State Circuits* **34** 456–68

[3] De Los Santos H J 2002 *RF MEMS Circuit Design for Wireless Communication* (London: Artech House)

[4] Tilmans H A C, De Raedt W and Beyne E 2003 MEMS for wireless communications: from RF-MEMS components to RF-MEMS-SiP *J. Micromech. Microeng.* **13** S139–63

[5] Varadan V K, Vinoy K J and Jose K A 2003 *RF MEMS and their Applications* (Pennsylvania State University, PA: Wiley)

[6] Pember A, Smith J and Kemhadjian H 1995 Study of the effect of boron doping on the aging of micromachined silicon cantilevers *Appl. Phys. Lett.* **66** 577–9

[7] Yong Y K and Vig J R 1989 Resonator surface contamination—a cause of frequency fluctuations? *IEEE Trans. Ultrason. Ferroelectr. Freq. Control* **36** 452–8

[8] Gallacher B J, Hedley J, Burdess J S and Harris A J 2003 Frequency tuning of silicon micromechanical cantilevers using laser ablation *Proc. NanoTech. Conf.* vol 1 pp 478–81

[9] Harvey E C 1997 Laser micromachining *Proc. IEE Coll. Micro. Eng. Tech.* vol 76 pp 3/1–3/2

[10] Tanaka K, Mochida Y, Sugimoto M, Moriya K, Hasegawa T, Atsuchi K and Ohwada K 1995 A micromachined vibrating gyroscope *Sensors Actuators* A **50** 111–5

[11] Syms R A and Moore D F 1999 Focused ion beam tuning of in-plane vibrating micromechanical resonators *IEE Electr. Lett.* **35** 1277–8

[12] Seabury C W, Cheung J T, Kobrin P H, Addison R and Havens D P 1995 High performance microwave air-bridge resonators *Proc. IEEE. Utrason. Symp.* vol 2 pp 909–11

[13] Wolf S and Tauber R N 1986 *Silicon processing for the VLSI Era. Process Technology* vol 1 (Sunset Beach, CA: Lattice Press) p 401

[14] Joachim D and Lin L 1999 Localized CVD of poly-crystalline silicon for post-fabrication processing *Proc. MEMS Symp. ASME. Int. Mech. Eng. Cong. Expos.* **1** 37–42

[15] Joachim D and Lin L 2003 Characterization of selective polysilicon deposition for MEMS resonator tuning *J. Microelectromech. Syst.* **12** 193–200

[16] Yao J J and MacDonald N C 1995 A micromachined, single-crystal silicon, tunable resonator *J. Micromech. Microeng.* **5** 257–64

[17] Lee K B and Cho Y-H 1998 A triangular electrostatic comb array for micromechanical resonant frequency tuning *Sensors Actuators* A **70** 112–7

[18] Adams S G, Bertsch F M, Shaw K A, Hartwell P G, Moon F C and MacDonald N C 1998 Capacitance based tuned resonators *J. Micromech. Microeng.* **8** 15–23

[19] Syms R A 1998 Electrothermal frequency tuning of folded and coupled vibrating micromechanical resonators *J. Microelectromech. Syst.* **7** 164–71

[20] Remtema T and Lin L 2001 Active frequency tuning for micro resonators by localized thermal stressing effects *Sensors Actuators* A **91** 326–32

[21] Wang K, Wong A-C, Hsu W-T and Nguyen C T-C 1997 Frequency trimming and *Q*-factor enhancement of micromechanical resonators via localized filament annealing *Proc. Int. Conf. Solid State Sens. Act.* **1** 109–12

[22] Johnstone R W and Parameswaran M 2002 Theoretical limits on the freestanding length of cantilevers produced by surface micromachining technology *J. Micromech. Microeng.* **12** 855–61

[23] Tas N, Sonnenberg T, Jansen H, Legtenberg R and Elwenspoek M 1996 Stiction in surface micromachining *J. Micromech. Microeng* **6** 385–97

[24] Knaap J and De Boer M P 2002 Mechanics of microcantilver beams subject to combined electrostatic and adhesive forces *J. Microelectromech. Syst.* **11** 754–64

[25] Micheal S F, Dirk W and Jordan M G 1998 The role of the Casimir effect in the static deflection and stiction of membrane strips in microelectromechanical systems (MEMS) *J. Appl. Phys.* **84** 2501–6

[26] Dequesnes M, Rotkin S V and Aluru N R 2002 Calculation of pull-in voltages for carbon-nanotube-based nanoelectromechanical switches *Nanotechnology* **13** 120–31

[27] Ashurst W R, Yau C, Carraro C, Maboudian R and Dugger M T 2001 Dichlorodimethylsilane as an anti-stiction monolayer for MEMS: a comparison to the octadecyltrichlosilane self-assembled monolayer *J. Microelectromech. Syst.* **10** 41–9

[28] Alley R L, Mai P, Komvopoulos K and Howe R T 1993 Surface roughness modification of interfacial contacts in polysilicon microstructures *Proc. 7th Int. Conf. Solid-State Sensors and Actuators (Transducers '93)* pp 288–91

[29] Teh W H, Luo J K, Graham M R, Pavlov A and Smith C G 2003 Near-zero curvature fabrication of miniaturized micromechanical Ni switches using electron beam cross-linked PMMA *J. Micromech. Microeng.* **13** 591–8

[30] Chan R, Lesnick R, Becher D and Feng M 2003 Low-actuation voltage RF MEMS shunt switch with cold switching lifetime of seven billion cycles *J. Microelectromech. Syst.* **12** 713–9

[31] Petersen K E 1978 Dynamic micromechanics of silicon: techniques and devices *IEEE Trans. Electron Devices* **10** 1241–50

[32] Pamidighantam S, Puers R, Baert K and Tilmans H A 2002 Pull-in voltage analysis of electrostatically actuated beam structures with fixed-fixed and fixed-free end conditions *J. Micromech. Microeng.* **12** 458–64

[33] Nemirovsky Y and Bochobza-Degani O 2001 A methodology and model for the pull-in parameters of electrostatic actuators *J. Microelectromech. Syst.* **10** 601–15

[34] Lanczos C 1949 *The Variational Principles of Mechanics* (Toronto: University of Toronto Press)

[35] Crandall S H 1968 *Dynamics of Mechanical and Electromechanical Systems* (Indianapollis, IN: Macmillan)

[36] Kierzenka J and Shampire L F 2002 *Solving Boundary Value Problems for Ordinary Differential Equations in Matlab With Bvp4c* (The MathWorks Inc.)

[37] Gao X-W and Davies T G 2002 *Boundary Element Programming in Mechanics* (Cambridge: Cambridge University Press)

[38] Bishop R E D and Johnson D C 1960 *The Mechanics of Vibration* (Cambridge: Cambridge University Press)

[39] Graeme F 1978 *Finite Element Galerkin's Methods for Differential Equations* (New York: Dekker)

[40] Vidar T 1933 *Galerkin Finite Element Methods for Parabolic Problems* (Berlin: Springer)